Macromolecules

Article

pubs.acs.org/Macromolecules

Water-Soluble Fluorescent Nanoparticles from Supramolecular Amphiphiles Featuring Heterocomplementary Multiple Hydrogen Bonding

Cheng-Wei Huang, Wen-Yu Ji, and Shiao-Wei Kuo*

Department of Materials and Optoelectronic Science, Center for Functional Polymers and Supramolecular Materials, National Sun Yat-Sen University, Kaohsiung 804, Taiwan

Supporting Information

ABSTRACT: We describe a facile strategy, involving bio-inspired noncovalent molecular recognition, for fabricating water-dispersible luminescent polymer dots without any ionic groups. We first synthesized the thymine-functionalized conjugated polymers PC-T and PTC-T through conventional Suzuki coupling polymerization and copper(I)-catalyzed alkyne/azide cycloaddition (CuAAC). These multiple-hydrogen-bonding materials exhibited distinct luminescent properties in protic and aprotic solvents as well as attractive thermal properties and stabilities; most importantly, they had the ability to pair with complementary base units. Next, we prepared the hydrophilic polymer PEG-A and examined its molecular recognition with PC-T and PTC-T through DNA-like adenine−thymine (A−T) base pairing. We used transmission electron microscopy (TEM) and dynamic light scattering (DLS) to determine the size distributions and dispersibilities of the resulting supramolecular micelles, which appeared as polymeric dots with high signal-to-background ratios through fluorescence microscopy. The PEG shells of these micelles functioned as biomimetic surfaces that sustained the biocompatibility for practical usage. Our results suggest that supramolecular self-assembly through specific nucleobase recognition appears to be a reliable process with which to apply conjugated polymers into, for example, modern biological analysis.

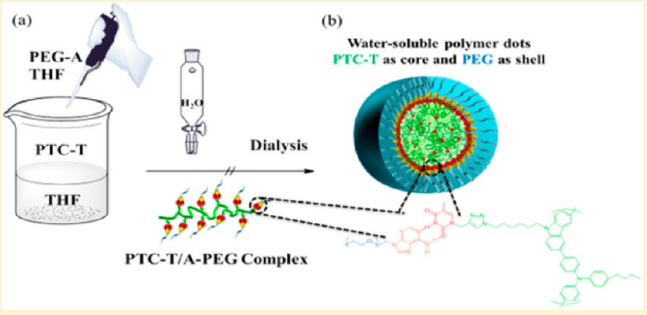

INTRODUCTION

Over the past two decades, many well-organized nanostructures have been fabricated from functional polymers. Self-assembly of these specific materials has provided a diverse array of colloidal architectures, including spherical micelles, vesicles, nanoribbons, and large compound micelles.[1−10] Among them, micellar structures have received considerable attention for their interesting behavior under various solvent conditions[11−15] and for their potential applications in pharmaceuticals and catalytic chemistry.[16−18] In particular, the hydrophilic shell of a micelle can function as a hydration barrier that stabilizes the entire system against the external medium.[19] The stability of micelles assembled from block copolymers is typically greater than that of small molecule micelles.[20] The morphologies of polymeric micelles can be tuned by varying the molecular weight and the solution parameters.[21,22] Accordingly, the flexibility of molecular design has opened up a variety of routes for preparing polymeric assemblies, thereby increasing scientific innovation for many fundamental and clinical purposes.

One of the most famous examples of self-assembly in nature is that performed by the nucleic acids (DNA, RNA), which are constructed from five basic nucleobases: adenine (A), cytosine (C), guanine (G), thymine (T), and uracil (U). The recognition of native nucleobase pairs (A−T, A−U, C−G) is particularly selective and specific and considerably stronger than most other noncovalent interactions.[23−28] Many nucleobase-functionalized polymers displaying interesting supramolecular characteristics have been prepared recently, taking advantage of this specific recognition behavior.[9] Rotello et al. suggested the term "plug and play" to describe systems with complementary base units located in separate molecular chains.[29] These systems can then be introduced into polymer/small molecule and polymer/polymer blends to extend the utility of the functional composite materials. Taking advantage of the dynamic interactions and adaptable features of plug-and-play systems, we can use many synthetic strategies to access smart polymers or biologically relevant substances that have the potential to become useful materials in diverse fields.[30−32]

Conjugated polymers are used extensively in materials science because of their semiconducting properties and light-emitting abilities.[33,34] A wide range of applications has been proposed for conjugated polymers in display technologies, organic photovoltaic devices, and sensors.[35] Furthermore, emissive polymer dots (Pdots) have been demonstrated as efficient fluorescent probes in the life sciences. Because of the ready tunability of the respective comonomers, conjugated

Received: July 17, 2017
Revised: September 2, 2017
Published: September 11, 2017

DOI: 10.1021/acs.macromol.7b01516
Macromolecules 2017, 50, 7091−7101

Scheme 1. Synthesis of (a) PC-T, (b) PTC-T, and (c) PEG-A

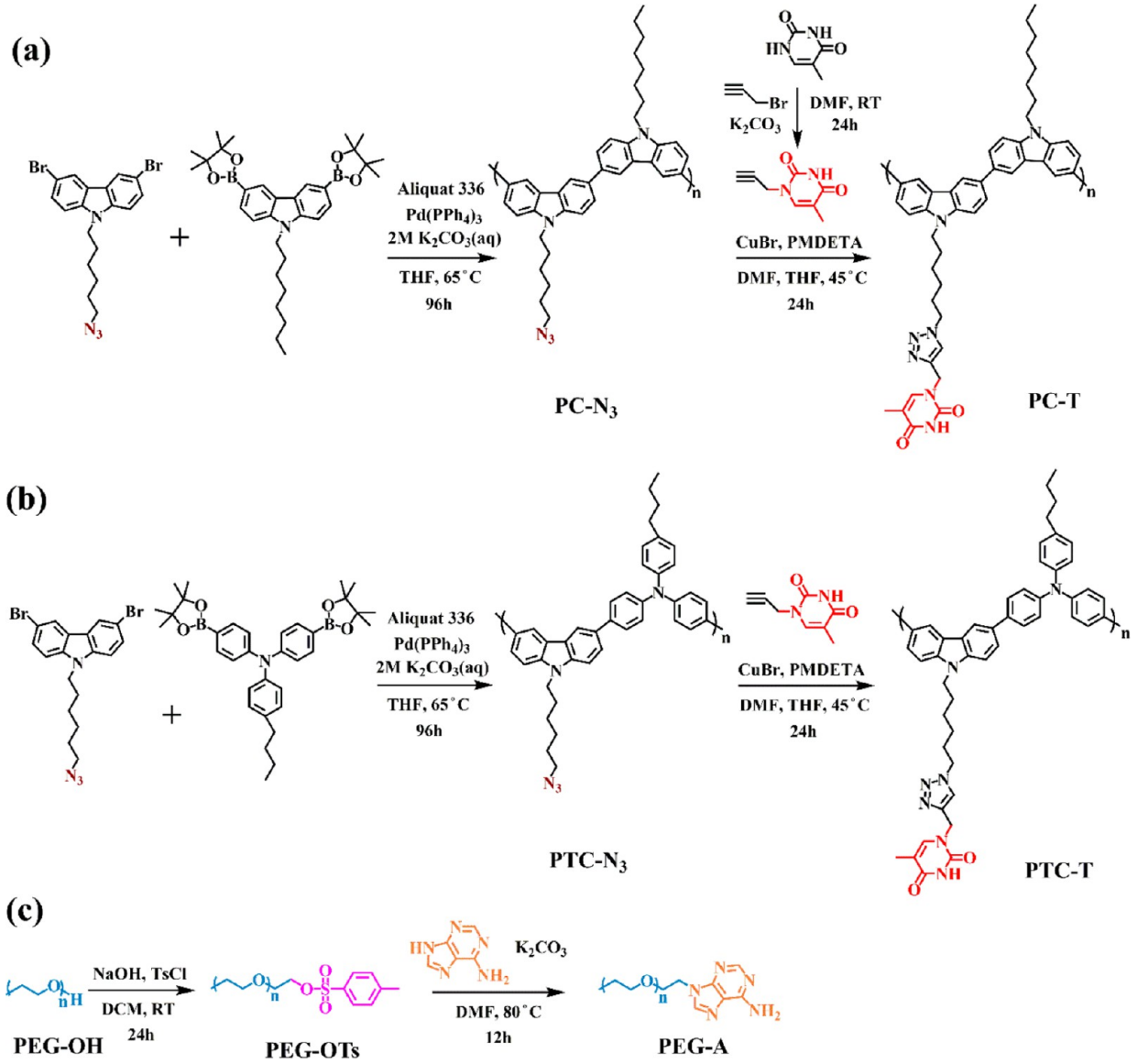

Pdots can exhibit high quantum yields and be simple to process.[33−36] Nevertheless, because solubility under aqueous conditions is a typical criterion for biological experiments, the inherent hydrophobicity of conjugated polymers has limited their development as fluorescent probes.[37,38] Herein, we describe a strategy, involving noncovalent interactions, that solves the solubility problem. We functionalized DNA base T units onto homo- and alternating-conjugated polymers, thereby enhancing the thermal properties through the physical cross-linked network supplied by T−T multiple hydrogen bonding. Thereafter, complementary A−T base pairing led to the formation of water-dispersible supramolecular micelles from two distinct types of polymers. The resulting supramolecular systems provided unique properties distinct from those of the precursor polymers. We used microscopy and light-scattering measurements to investigate the morphologies of these polymeric micelles, which were capable of emitting light under photoexcitation. The photoluminescence (PL) characteristics were examined through PL spectroscopy and observed under fluorescence microscopy. Our results suggest the possibility of using supramolecular micelles as polymer dots. We checked their biocompatibility through cell viability experiments, observing little cytotoxicity even through the materials incorporated aromatic-rich conjugated polymers. Through the methodology proposed in this study we have found that conjugated polymeric micelles can act as polymer dots, suggesting the increased practical use of these interesting materials.

EXPERIMENTAL SECTION

Materials. Organic solvents were purchased from TEDIA (USA). Dimethylformamide (DMF) was distilled over CaH_2; tetrahydrofuran (THF) was heated under reflux with sodium lumps and distilled prior to use. Copper(I) bromide was stirred with acetic acid at room temperature, filtered off, washed with MeOH and diethyl ether, and then dried under vacuum. The deionized water was prepared from Milli-Pore machine (Hamburg, Germany). Poly(ethylene glycol) (PEG; M_n = 2000; Sigma-Aldrich) was subjected to azeotropic distillation in dry toluene to remove water. 3,6-Dibromo-9*H*-carbazole (**1**), 4-butyl-*N*,*N*-bis(4,4,5,5-tetramethyl-1,3,2-dioxaborolane-4-phenyl)aniline, 9-(6-bromohexyl)-3,6-dibromo-9*H*-carbazole (**2**), 9-(6-azidohexyl)-3,6-dibromo-9*H*-carbazole (**3**), the precursor polymer PTC-N_3, and propargyl thymine (PT) were prepared according to previous reports (Scheme S1).[39,40] PEG-OTs and PEG-A were also synthesized according to previously

DOI: 10.1021/acs.macromol.7b01516
Macromolecules 2017, 50, 7091−7101

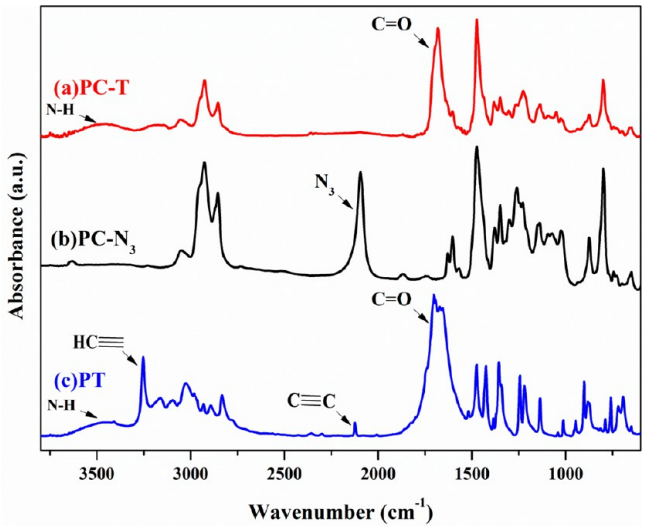

Figure 1. FTIR spectra of (a) PC-T, (b) PC-N_3, and (c) PT.

reported procedures, as displayed in Scheme 1c.[41] All other reagents were obtained from Sigma-Aldrich, TCI, and Showa and used without further purification.

Synthesis of 3,6-Dibromo-9-octyl-9*H*-carbazole (4). 3,6-Dibromo-9*H*-carbazole (3.50 g, 10.7 mmol) and K_2CO_3 (2.98 g, 21.5 mmol) were placed in a flame-dried flask. Acetonitrile (45 mL) was added, and then the mixture was stirred for 30 min. Bromooctane (20.66 g, 107 mmol) was added, and then the mixture was heated at 95 °C for 36 h. The mixture was filtered and distilled to remove the solvent and residual bromooctane. Recrystallization of the residue (petroleum ether) gave a white solid (3.7 g, 80%). T_m = 80 °C. ^{1}H NMR (500 MHz, $CDCl_3$, δ): 8.14 (s, 2H, ArH), 7.55 (d, 2H, J = 8.8 Hz, ArH), 7.27 (d, 2H, J = 8.8 Hz, ArH), 4.23 (t, 2H, J = 7.0 Hz, CH_2), 1.82 (m, 2H, CH_2), 1.39−1.15 (m, 10H, CH_2), 0.86 (t, 3H, J = 6.5 Hz, CH_3). ^{13}C NMR (500 MHz, $CDCl_3$, δ): 140.0, 129.8, 124.1, 123.9, 112.6, 110.9, 43.3, 33.8, 32.6, 28.8, 27.9, 26.5.

Synthesis of 9-Octyl-3,6-bis(4,4,5,5-tetramethyl-1,3,2-dioxaborolan-2-yl)-9*H*-carbazole (5). *n*-Butyllithium (2.5 M in hexane; 5.7 mL, 14.3 mmol) was added dropwise to a solution of 3,6-dibromo-9-octyl-9*H*-carbazole (2.5 g, 5.72 mmol) in anhydrous THF (100 mL) at −78 °C, and then the mixture was stirred at −78 °C for 1 h. 2-Isopropoxy-4,4,5,5-tetramethyl-1,3,2-dioxaborolane (3.19 g, 17.15 mmol) was added, and then the reaction was left overnight. The THF was evaporated, and the residue was dissolved in $CHCl_3$ and extracted with brine. The organic phase was dried ($MgSO_4$) and concentrated. The crude product was purified through column chromatography (EtOAc/hexanes, 1:10) to give a colorless oil. ^{1}H NMR (500 MHz, $CDCl_3$, δ): 8.70 (s, 2H, ArH), 7.94 (d, 2H, J = 8.2 Hz, ArH), 7.41 (d, 2H, J = 8.2 Hz, ArH), 4.31 (t, 2H, J = 7.0 Hz, CH_2), 1.87 (m, 2H, CH_2), 1.42 (s, 24H, CH_3), 1.38−1.19 (m, 10H, CH_2), 0.88 (t, 3H, J = 6.9 Hz, CH_3). ^{13}C NMR (500 MHz, $CDCl_3$, δ): 143.4, 132.6, 128.7, 123.4, 108.7, 108.6, 83.9, 43.3, 0.31.9, 29.5, 29.3, 29.0, 27.3, 25.0, 22.7, 14.1.

Synthesis of PC-N_3. Aliquat 336 (several drops) and aqueous K_2CO_3 (2 M, 1 mL) were added to a solution of the carbazole monomer **3** (0.30 g, 0.73 mmol) and **5** (0.40 g, 0.73 mmol) in anhydrous THF (5 mL) in a flame-dried Schlenk tube. The mixture was subjected to three freeze/pump/thaw cycles and then heated under reflux at 65 °C for 96 h. The resulting polymer was precipitated by pouring into cold MeOH; it was redissolved in $CHCl_3$ and passed through a short column of Celite to remove the catalyst. After Soxhlet extraction with MeOH and acetone, a yellow powder was recovered (55% yield). ^{1}H NMR (500 MHz, $CDCl_3$, δ): 8.55 (br, ArH), 7.88 (br, 2H, ArH), 7.48 (br, ArH), 4.31 (br, CH_2), 3.21 (br, CH_2N_3) 1.92 (br, CH_2), 1.51−1.06 (br, CH_2), 0.88 (br, CH_3).

Synthesis of PC-T. A mixture of propargyl thymine (0.27 g, 1.7 mmol) in 15 mL of anhydrous DMF, PC-N_3 (0.30 g, 0.55 mmol of N_3 groups) in 15 mL of anhydrous THF, and Cu(I)Br (4 mg) was subjected to a freeze/pump/thaw cycle. PMDETA (5 μL) was transferred into the reaction vessel, and then the mixture was heated at 45 °C for 24 h. The mixture was passed through an aluminum oxide column and then dialyzed with dilute HCl and MeOH. Several cycles of reprecipitation in MeOH provided an off-white polymeric product (95% yield). ^{1}H NMR (500 MHz, $CDCl_3$, δ): 9.30 (br, NH), 8.88 (br, ArH), 7.84 (br, ArH), 7.44 (br, ArH), 4.73 (br, CH_2), 4.43−3.80 (br, C=CCH_2N, NCH_2), 1.92 (br, CH_2), 1.64 (s, thymine CH_3), 1.49−1.00 (br, CH_2), 0.86 (br, CH_3).

Synthesis of PTC-T. PTC-N_3 was synthesized from the carbazole monomer **3** and the TPA monomer 4-butyl-*N*,*N*-bis(4,4,5,5-tetramethyl-1,3,2-dioxaborolane-4-phenyl)aniline. Using a procedure similar to that described for PC-T, PTC-T was synthesized from PTC-N_3 and propargyl thymine. A pale yellow powder was recovered (95% yield). ^{1}H NMR (500 MHz, DMSO-d_6, δ): 11.26 (br, NH), 8.53 (br, ArH), 7.61 (br, ArH), 7.00 (br, ArH), 4.81 (br, CH_2), 4.49−3.95 (br, C=CCH_2N, NCH_2), 1.82−1.42 (br, CH_2), 1.39−0.97 (br, CH_2, thymine CH_3), 0.95−0.75 (br, CH_2, CH_3).

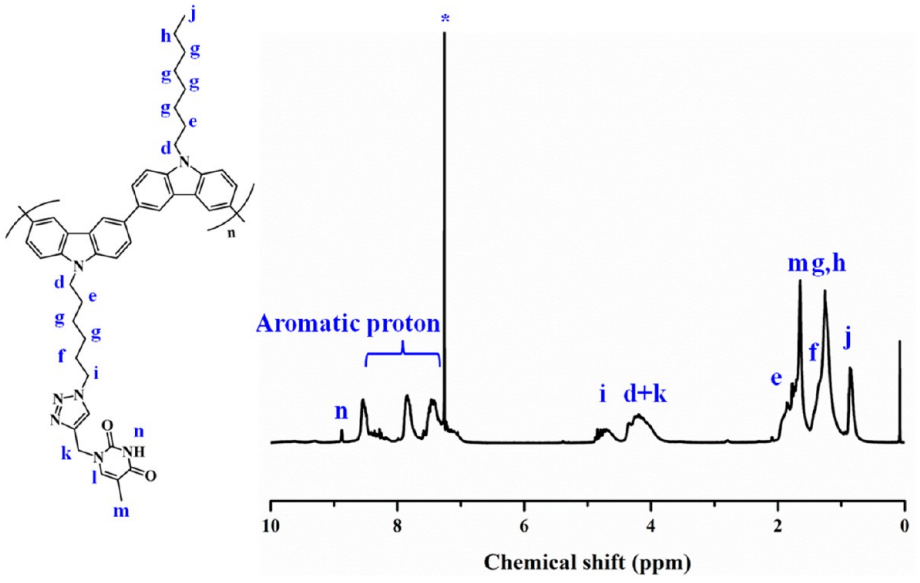

Figure 2. ^{1}H NMR spectrum of PC-T in $CDCl_3$ (*signal from the solvent).

DOI: 10.1021/acs.macromol.7b01516
Macromolecules 2017, 50, 7091−7101

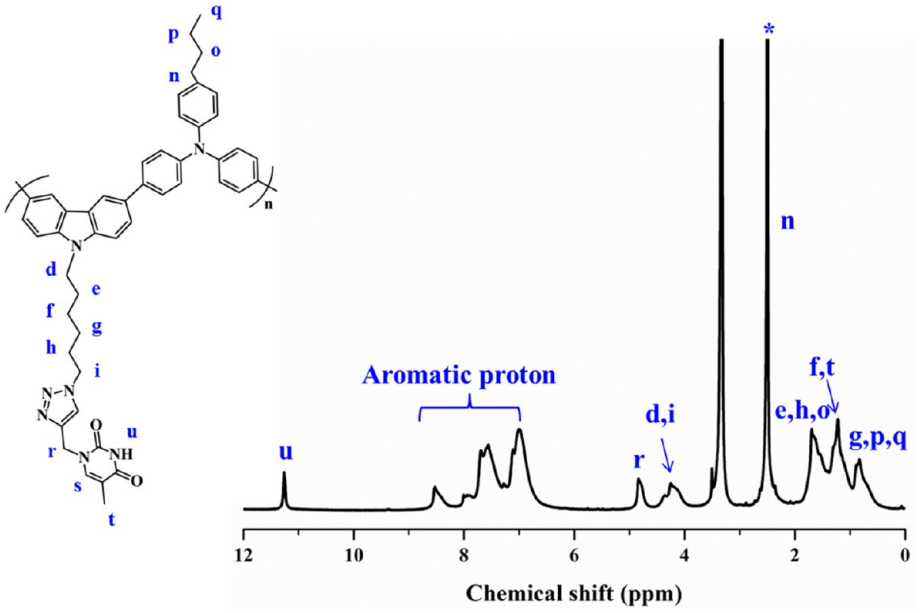

Figure 3. ^{1}H NMR spectrum of PTC-T in DMSO-d_6 (*signal from the solvent).

Table 1. Characterization Data for the Polymers Used in This Study

polymer	M_n[a]	PDI[a]	T_d[b] (°C)	char yield[b] (%)	T_g[c] (°C)
PC-N_3	3620	1.45	324.2	60	99.5
PTC-N_3	8260	1.45	269.7	55	109.4
PC-T	9400	1.29	346.7	40	145.3
PTC-T	16800	1.42	359.1	48	161.7

[a]Calculated using GPC: THF eluent for PC-N_3 and PTCN_3, DMF for PC-T and PTC-T. [b]Calculated using TGA; T_d was measured as the temperature of 5 wt % decomposition. [c]Calculated using DSC.

Supramolecular Dots. The T-containing polymer PC-T (or PTC-T) was dissolved in THF, and then a solution of PEG-A in THF was added slowly to form a 1:1 molar ratio supramolecular mixture, which was stirred at room temperature for 1 h. The THF solution was then treated with various amounts of deionized water and stirred for another 1 h. The mixture was dialyzed against deionized water for 48 h to remove the organic solvent and lyophilized to recover a film-like solid, which was redissolved in deionized water for further characterization.

Cell Viability. Cell viability was measured using a colorimetric assay in 96-well plates with 2-(4-iodophenyl)-3-(4-nitrophenyl)-5-(2,4-disulfophenyl)-2*H*-tetrazolium monosodium salt (WST-1) reagent. Samples were dispersed with Dulbecco's modified Eagle's medium (DMEM) or Ham's F-12K (Kaighn's) medium and cultivated with rat liver clone 9 cells for 24 h. WST-1 was added, and the cells were incubated for an additional 2 h. The medium containing the unreacted dye was removed carefully, and the cell viability was measured at a wavelength of 450/690 nm.

Characterization. ^{1}H and ^{13}C nuclear magnetic resonance (NMR) spectra of samples were recorded in $CDCl_3$ or DMSO-d_6 using an Agilent Unity Inova 500 spectrometer, operated at 500 and 125 MHz, respectively. Molecular weights and polydispersity indices (PDIs) were measured using a Waters 510 gel permeation chromatography system equipped with three Ultrastyragel columns (100, 500, and 1000 Å) connected in series. DMF was the eluent (flow rate: 0.8 mL min^{-1}; 50 °C). The DMF-insoluble polymers were characterized with a THF as the eluent equipped with a JASCO RI-2031 detector and a Styragel HR4 column. The system was calibrated using polystyrene (PS) standards and measured with a refractive index detector. Fourier transform infrared (FTIR) spectra were recorded using a Bruker Tensor 27 FTIR spectrometer; samples were prepared using the regular KBr disk method, and 32 scans were recorded at room temperature at a resolution of 1 cm^{-1}. A TA Q-50 thermogravimetric analyzer was used to measure the thermal stabilities of the samples under a N_2 atmosphere. The sample (ca. 5 mg) was placed in a Pt cell and heated at a rate of 20 °C min^{-1} from 30 to 800 °C under a N_2 flow rate of 60 mL min^{-1}. Differential scanning calorimetry (DSC) was performed using a TA Instruments Q-20 apparatus under an atmosphere of dry N_2; the samples (3−5 mg) were sealed in an aluminum pan and scanned from −80 to +150 °C at a rate of 10 °C min^{-1}. Dynamic light scattering (DLS) was performed using a Brookhaven Instrument Corporation 90-plus apparatus with a scattering angle of 173°. PL emission spectra were recorded in solution at room temperature using a Hitachi F-4500 fluorescence spectrometer and a monochromatized Xe light source. The concentration of each sample was 5 × 10^{-4} M; measurement from 200 to 800 nm was performed at a scan rate of 240 nm min^{-1}. TEM images were recorded using a JEOL-2100 transmission electron microscope operated at an accelerating voltage of 200 kV. Fluorescence images were acquired using an inverted optical microscope (IX-71, Olympus) and a Xe arc lamp (Lambda LS, Sutter Instrument). The excitation light was filtered through a bandpass filter (FF01-370/36), reflected by a dichroic filter (Di01-R405, Semrock), and focused onto the sample through an oil-immersed 100× objective. The fluorescence signal was passed through the dichroic filter and an

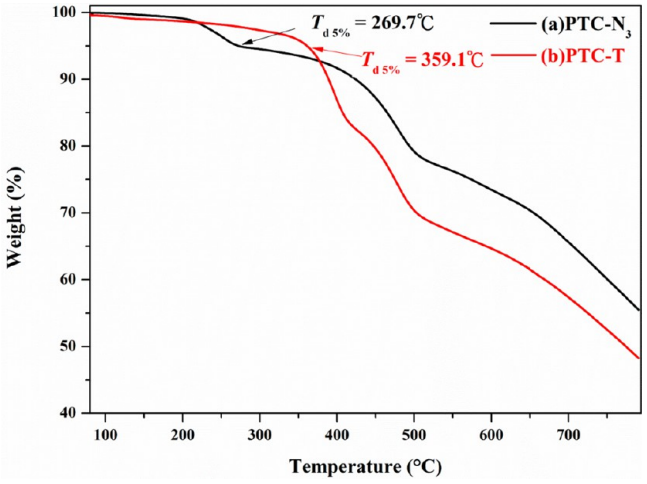

Figure 4. TGA thermograms of (a) PTC-N_3 and (b) PTC-T.

DOI: 10.1021/acs.macromol.7b01516
Macromolecules 2017, 50, 7091−7101

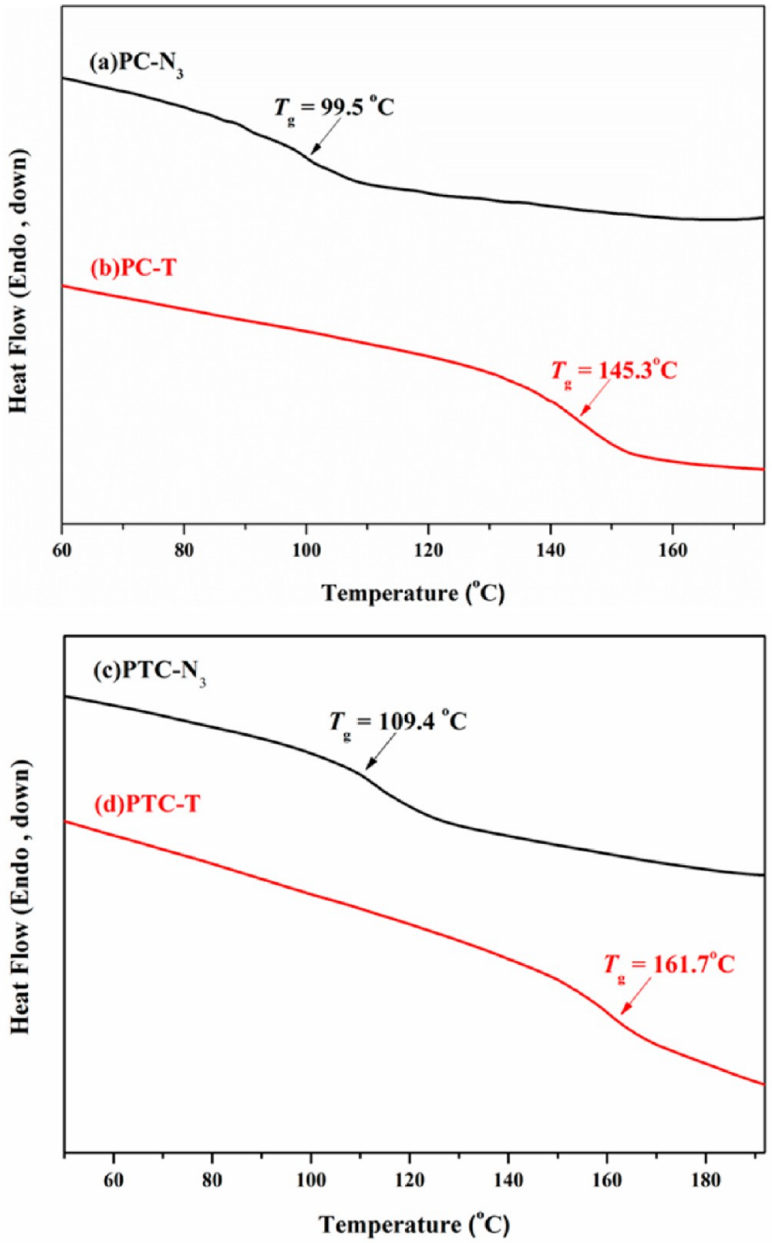

Figure 5. DSC thermograms of (a) PC-N_3, (b) PC-T, (c) PTC-N_3, and (d) PTC-T.

Table 2. Thermal Properties of Supramolecular Materials Used in This Study

sample	T_m[a] (°C)	T_c[a] (°C)	T_g[a] (°C)
PC-T			145.2
PEG-A	53.6	24.6	
PC-T:PEG-A	51.8	17.7	119.0

[a]Measured using DSC.

emission filter (BLP01-405R) and then recorded by a charge-coupled device (CCD; iXon DV885, Andor).

RESULTS AND DISCUSSION

Synthesis and Characterization of PC-T and PTC-T. Scheme 1 displays the synthesis of the T-contained polymers. 3,6-Dibromo-9-octyl-9*H*-carbazole (**4**) and 9-octyl-3,6-bis(4,4,5,5-tetramethyl-1,3,2-dioxaborolan-2-yl)-9*H*-carbazole (**5**) were synthesized using procedures similar to those we have described

Scheme 2. (a) Preparation of PCT-T/A-PEG Complex and (b) Water-Soluble Polymer Dots with Multiple Hydrogen Bonding Interactions between PCT-T and A-PEG

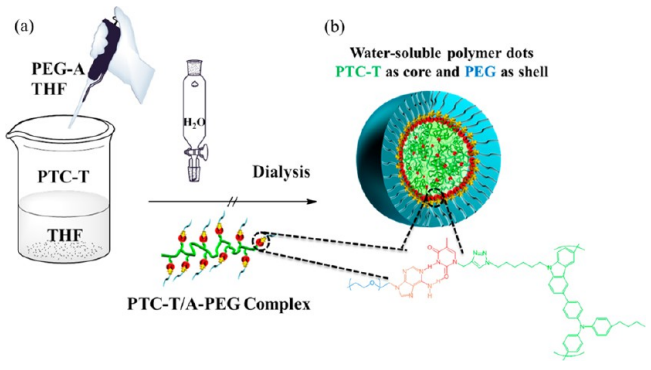

DOI: 10.1021/acs.macromol.7b01516
Macromolecules 2017, 50, 7091−7101

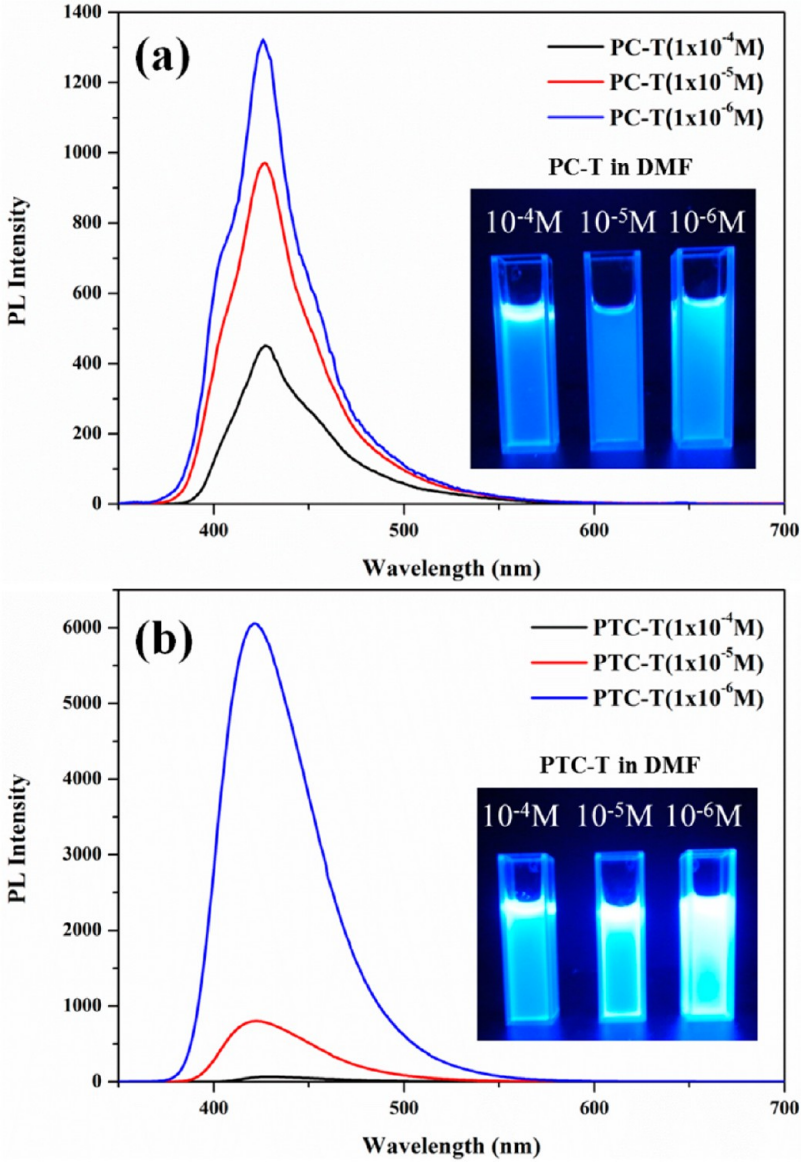

Figure 6. PL spectra of PTC-T at various concentrations. Inset: photographs of the resulting solutions.

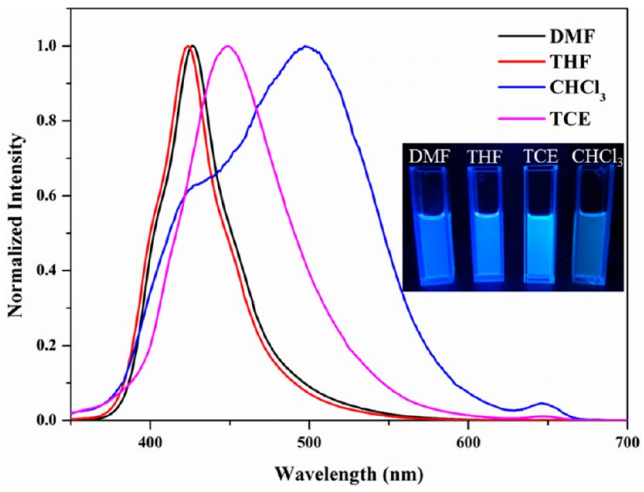

Figure 7. PL spectra of PC-T in various solvents. Inset: photographs of the resulting solutions.

previously.[16] The ^{1}H and ^{13}C NMR spectra of the monomers **4** and **5** are presented in Figures S1 and S2. PC-N_3 was first synthesized from the carbazole monomers. The characteristic peak of the side chain azido groups of PC-N_3 appeared at 2095 cm^{-1} (Figure 1), whereas the C≡C signal of propargyl thymine appeared at 2120 cm^{-1}. Both of these signals disappeared after postfunctionalization of PC-N_3 to form PC-T through a click reaction.

Further evidence for the successful synthesis was evident in the NMR spectra of the polymers. In the ^{1}H NMR spectra, the signal of the protons next to the side chain azido groups appeared at 3.21 ppm for PC-N_3 (Figure S3) and shifted to 4.73 ppm to reflect the formation of the 1,2,3-triazole groups (Figure 2).

In addition, the characteristic signals of a T moiety were observed at 9.30 (NH) and 1.64 ppm (CH_3), while the signal for the alkyne unit of propargyl thymine (at 2.43 ppm) disappeared completely. Similar trends were evident for PTC-N_3 and PTC-T (Figure S4 and Figure 3), with no disruption of the chemical shifts of the aromatic and aliphatic protons. We used

DOI: 10.1021/acs.macromol.7b01516
Macromolecules 2017, 50, 7091−7101

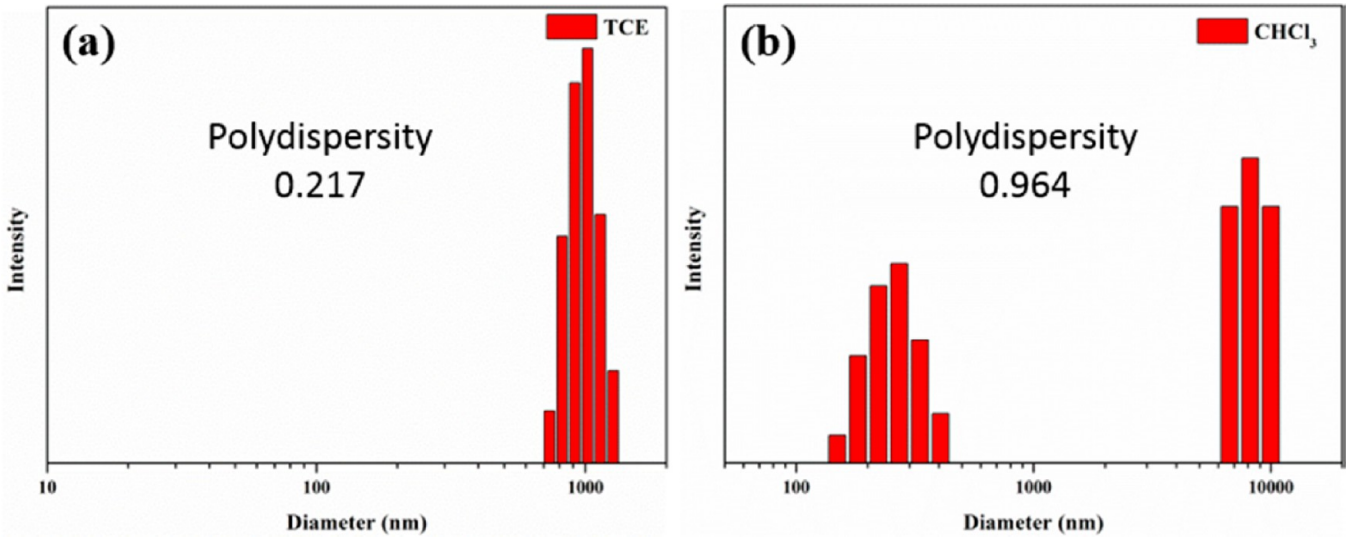

Figure 8. DLS spectra of PC-T in (a) TCE and (b) $CHCl_3$ at 10^{-6} M.

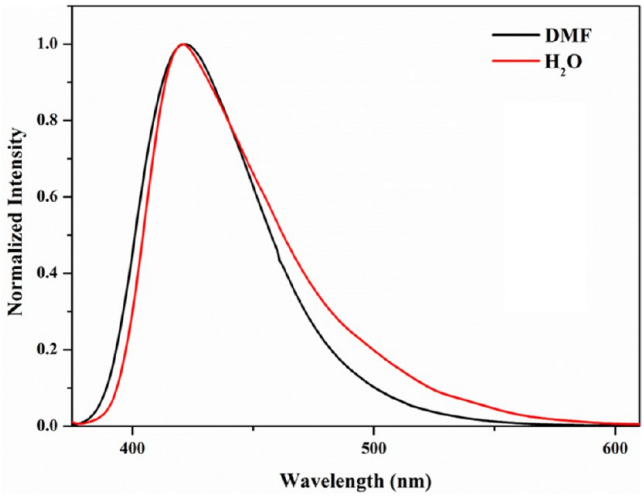

Figure 9. PL spectra of PTC-T in DMF and of PTC-T:PEG-A polymer dots in H_2O.

GPC to calculate the molecular weight information (Table 1). Increases in the values of M_n and M_w suggested that side-chain grafting had contributed to increasing the entire molecular weight. Taking all of these results together, we conclude that postfunctionalization of the conjugated polymers had been conducted successfully through click reactions.

Thermal Properties and Stability of T-Functionalized Conjugated Polymers. We used TGA thermograms to measure the thermal properties of the conjugated polymers (Figure 4, Figure S5, and Table 1). The TGA curves revealed early decomposition at 324.2 and 269.7 °C for PC-N_3 and PTC-N_3, respectively. The first-stage decomposition provided a weight loss of approximately 5%, suggesting that a reaction occurred with the reactive azide functionalities. Organic azides readily form nitrene intermediates, generating N_2 gas at the same time. The active nitrene group can attack neighboring atoms and, thus, form chemically cross-linked networks, resulting in char yields higher than those of other common materials. In contrast, the T-functionalized conjugated polymers had significantly increased values of T_d, presumably because of the physically cross-linked network provided by strong T−T hydrogen bonding and the lack of azido groups after performing the click reaction.

We also used DSC to examine the enhancement in the thermal properties (Figure 5). During the heating and cooling processes, we did not observe any obvious melting or crystallization peaks, presumably because of the poor packing ability of the arylamine structure due to the 3D structure and a deficiency of planarity. Nevertheless, the rigid conjugated backbone contributed to high values of T_g of approximately 100 °C for both PC-N_3 and PTC-N_3. The glass transition temperature was more difficult to reach after functionalization with the T units. The value of T_g increased by 40−50 °C after performing the click reaction—evidence that strong interactions between T units may have greatly restricted the segmental motion of the polymer backbone, leading to a more stable morphology and sustainability against high temperature.

Molecular Recognition of PC-T/PEG-A. Thymine-functionalized materials can exhibit excellent properties arising from their self-association hydrogen bonding. In addition, T moieties have the ability to form multiple hydrogen bonds with complementary base units. The heterocomplementary A−T base pairs can be used to fabricate novel supramolecular architectures through molecular recognition. For this reason, in this study we examined the behavior of the PC-T/PEG-A supramolecular complex. After simple blending, the supramolecular complex was recovered and subjected to DSC (Figure S6 and Table 2). Formation of the supramolecular complex affected the original packing of the PEG chains and resulted in shifts in the values of T_m and T_c. We also observed a decrease in the value of T_g from 145.2 °C (for PC-T) to 119.0 °C (for the complex), owing to the presence of the flexible PEG chains. Therefore, a supramolecular complex combining the properties of PC-T or PTC-T and PEG-A had been prepared through A−T molecular recognition (Scheme 2).

PL Properties. We recorded PL spectra of the conjugated polymer at various concentrations to understand its interactions. Figure 6a presents the PL spectra of PC-T in DMF. The intensity of the PL decreased upon increasing the concentration, indicating that PC-T could be classified as displaying an aggregation-caused quenching (ACQ) type of luminescence. Although PTC-T also exhibited an ACQ type of emission (Figure 6b), the intensity of PTC-T at 10^{-6} M was approximately 5 times that of PC-T. This phenomenon can be explained by considering the distinct molecular structure in the polymer

DOI: 10.1021/acs.macromol.7b01516
Macromolecules 2017, 50, 7091−7101

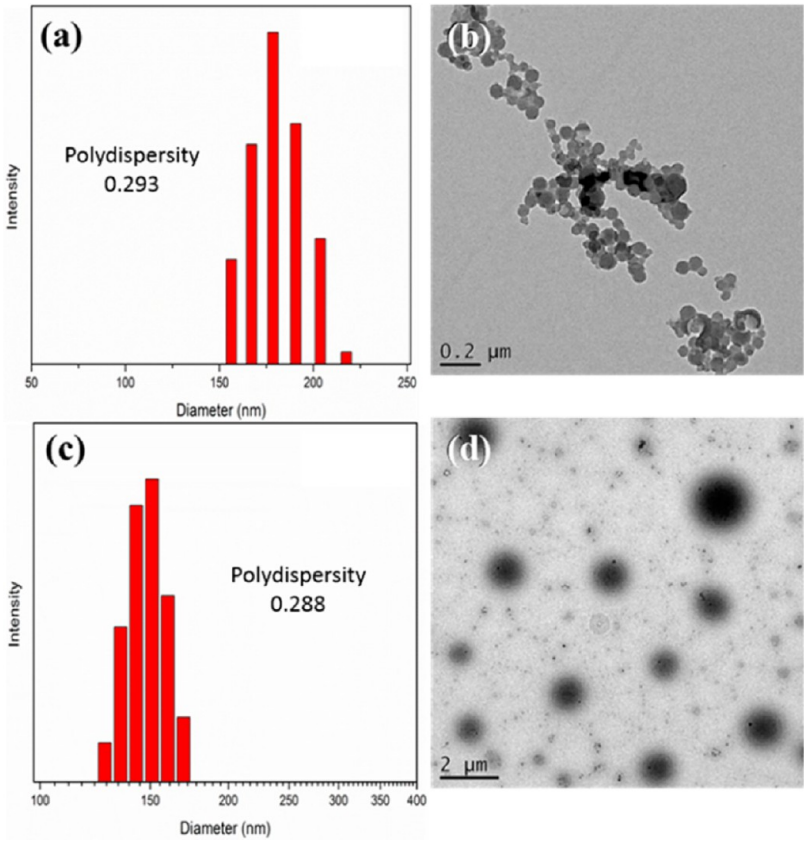

Figure 10. (a, c) DLS spectra and (b, d) TEM images of PTC-T:PEG-A polymer dots in (a, b) H_2O and (c, d) PBS (pH 7).

backbone. Because triphenylamine (TPA) has a bulky structure and relatively high quantum efficiency, the alternating copolymer PTC-T should emit more strongly than the carbazole-constructed PC-T homopolymer. Another critical issue in these hydrogen-bonded polymers is the solvent effect. For clarity, we measured the PL spectra of all of the polymers in various solvents at a concentration of 10^{-6} M. Figure 7 reveals broader emission signals and shifted main peaks for the samples in $CHCl_3$ and 1,1,2,2-tetrachloroethane (TCE) compared with those in DMF and THF.

We suspect that protic solvents, such as DMF and THF, readily formed hydrogen bonds with the T units of PC-T and disrupted the physically cross-linked structures formed through T−T interactions. The better solubility, compared with that in aprotic solvents ($CHCl_3$, TCE) that did not interact with the T units, suppressed aggregate formation and retained the original emission. Aggregation in TCE resulted in an eximeric dominant emission; this phenomenon was most evident in $CHCl_3$. DLS measurements provided consistent results (Figure 8).

No obvious aggregation occurred in the protic solvents, but one signal for aggregation was found near 1000 nm in the TCE solution. In contrast, we observed two different scales of aggregation and a larger polydispersity (0.964) in the $CHCl_3$ solution. The relatively higher PDI may cause by the two distributions of aggregates, suggesting that PC-T had relatively poor solubility in this solvent. The alternating polymer PTC-T exhibited similar trends in these solvents (Figure S7). Furthermore, the higher quantum efficiency of PTC-T meant that the emission intensity was higher in the DMF solution than in the TCE solution at the same concentration due to lower degree of aggregate formation in DMF and the superior solubilization. DLS analysis of PTC-T also provided evidence for the scale of aggregation being greater in the aprotic TCE solution. Taking these observations together, we conclude that the T-functionalized conjugated polymers had better solubility in protic solvents. Thus, the selection of the solvent type must be taken into consideration when applying these special materials.

PL and Morphologies of Water-Soluble Polymer Dots. The most important aspect of postfunctionalization with T units is the flexibility in material construction. That is, even if most conjugated polymers are hydrophobic due to their low polarity and carbon-based main-chain structure, they can become hydrophilic after exploiting the nucleobase. In this study, we prepared water-soluble polymer dots through heterocomplementary hydrogen bonding between luminescent polymers and the hydrophilic polymer PEG. The PL spectra of the original PTC-T emission in DMF and of PTC-T:PEG-A in H_2O are presented in Figure 9; the spectra of PC-T:PEG-A in H_2O are displayed in Figure S8. The spectra of PTC-T:PEG-A exhibited a shifted and broadened emission in water compared with the original emission in DMF. When the conjugated polymer started to form polymer dots, the polymer backbone tended to fold into a compact structure, potentially leading to a slight increase in the possibility of $\pi-\pi$ interactions and extending the conjugation length of the polymer.[42] On the other hand, the association process of A−T base pairs can promote the interchain interactions of molecules and of chromophoric segments in solution.[43,44] Thus, the PL spectra provided evidence for the formation of polymer dots.

To gain clearer insight, we used DLS to examine the morphologies of the complexed species. The PC-T:PEG-A polymer dots exhibited a mean diameter of 144 nm in water and

DOI: 10.1021/acs.macromol.7b01516
Macromolecules 2017, 50, 7091−7101

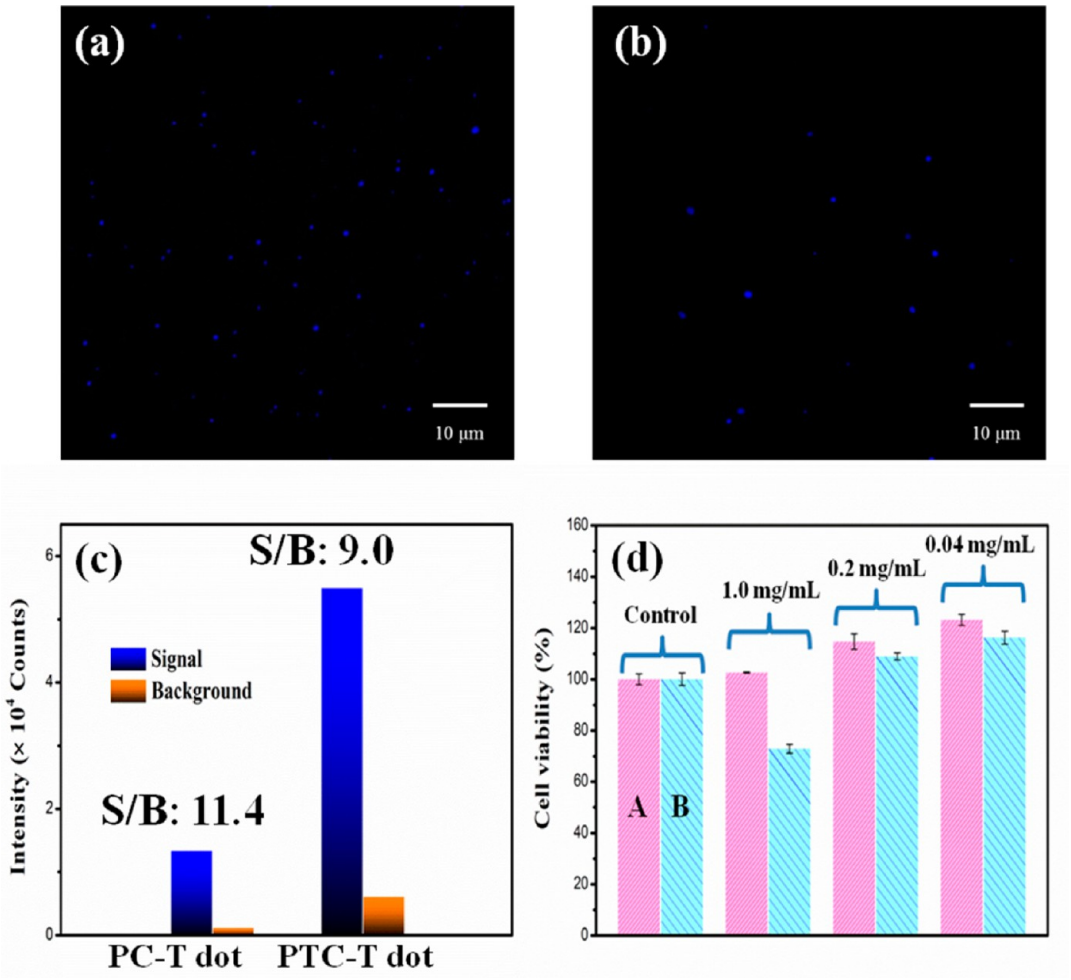

Figure 11. (a, b) Fluorescence microscopy images of (a) PC-T and (b) PTC-T; (c) signal and background intensity for Pdots under the same excitation conditions; (d) cell viability of clone 9 cells against (A) PC-T dots and (B) PTC-T dots at various concentrations.

polydispersity of 0.293 (Figure 10a). TEM analysis (Figure 10b) was consistent with the light scattering data. The presence of nanoparticles with dimensions of less than 200 nm suggested the successful formation of micellar-like supramolecular structures. The observation of PC-T:PEG-A under the same conditions (Figure S9) revealed a mean diameter of 179 nm in water (polydispersity: 0.268). The assemblies were also formed in PBS (pH 7)—that is, under conditions similar to those found in the human body. In the PBS solution, however, the micelles were larger and less aggregation occurred, presumably because of the difference in surface tension between water and the buffer solution. In addition, the ions present in the buffer solution could adsorb onto the shells of the micelles and, thus, provide a repulsive force to prevent aggregate formation. It was found that PDI's for PC-T:PEG-A and PTC-T:PEG-A micelles were at the same scale, which may be explained by the similar formation mechanism via complementary hydrogen bonding. In both the water and PBS solutions, the sizes of the micelles determined through TEM analysis were smaller than those determined using DLS, presumably because of the swelling effect in the solution state.

To explore their potential applications, we used fluorescence microscopy to investigate the supramolecular polymer dots. Figure 11a,b presents typical fluorescence images of the PC-T dots and PTC-T dots, obtained under identical excitation and acquisition conditions. The images acquired under the low excitation power (1 mW) of a 395 nm laser revealed clear bright spots, indicating that high emission intensities can be obtained from supramolecular polymer dots. In addition, we calculated high signal-to-background (S/B) ratios of 11.4 and 9.0 for the PC-T dots and PTC-T dots, respectively (Figure 11c). The relatively higher S/B ratio of the PC-T dots may have resulted from a small effective excitation volume, which can minimize interference from autofluorescence and excitation outside the laser focal volume.[45,46] Such a high S/B ratio may facilitate fluorescence detection at a low excitation power. To explore their potential applications in biomedicine, we evaluated the biocompatibility of the supramolecular polymer dots through an MTT assay using clone 9 rat liver normal cells. The cell viability of these polymer dots (Figure 11d) suggested little cytotoxicity, except for the PTC-T dots at high concentration. The relatively lower cell viability of the PTC-T dots may have resulted from the cytotoxicity of the TPA groups on the polymer backbone. It has been reported that TPA units may undergo nuclear translocation from the cytoplasm in living cells within the period of photoexcitation.[47] This effect is, however, negligible under daylight or in a dark environment when the concentration is less than 30 μm.[48] This trend was also reflected in our experiment, where very little cytotoxicity was evident in the diluted sample. In addition, our PC-T dots did not exhibit any obvious decrease in cell viability upon increasing the concentration, indicating good biocompatibility, presumably the

DOI: 10.1021/acs.macromol.7b01516
Macromolecules 2017, 50, 7091−7101

result of noncovalent functionalization with the biocompatible PEG component.

CONCLUSION

We have prepared the T-functionalized conjugated homopolymer PC-T and alternating polymer PTC-T through Suzuki coupling polymerization and a click reaction. These supramolecular polymers exhibited enhanced thermal properties and stability. Differences in the PL in various solvents revealed the role of the side chain T groups. Molecular recognition between T and A units increased the water solubility of these conjugated polymers. Supramolecular micelles were constructed from the conjugated polymers and a hydrophilic PEG polymer, as evidenced using microscopy and light scattering. The heterocomplementary multiple hydrogen bonding in aqueous solutions resulted in supramolecular micelles within a narrow size distribution, with diameters of less than 200 nm. We examined these micelles for their suitability for use as polymer dots. Fluorescence microscopy revealed good water dispersibility and strong signal-to-background ratios. Furthermore, cell viability evaluations demonstrated that the polymer dots were biocompatible, suggesting potential utility in bioimaging. The facile noncovalent complexation approach reported herein appears to be a useful strategy for preparing biocompatible fluorescent materials containing conjugated polymers, possibly expanding the biomedical applications of such materials.

ASSOCIATED CONTENT

Supporting Information

The Supporting Information is available free of charge on the ACS Publications website at DOI: 10.1021/acs.macromol.7b01516.

Figures S1−S9 (PDF)

AUTHOR INFORMATION

Corresponding Author

*E-mail: kuosw@faculty.nsysu.edu.tw (S.-W.K.).

ORCID

Cheng-Wei Huang: 0000-0003-1891-8031

Shiao-Wei Kuo: 0000-0002-4306-7171

Notes

The authors declare no competing financial interest.

ACKNOWLEDGMENTS

This study was supported financially by the Ministry of Science and Technology, Taiwan, under Contracts MOST103-2221-E-110-079-MY3 and MOST102-2221-E-110-008-MY3. We thank Professor Jui-Hung Hsu (Department of Materials and Optoelectronic Science, National Sun Yat-Sen University) for help with the fluorescence microscope and Mr. Hsien-Tsan Lin (Regional Instruments Center, National Sun Yat-Sen University) for assistance with the TEM. We also thank Professor Hsueh-Ling Cheng, Mr. Chun-Hsien Yu (National Pintung University of Science and Technology) for help with the cytotoxicity experiments and Professor Shi-Yie Cheng (Department of Life Sciences, National University of Kaohsiung) for the further discussions.

REFERENCES

(1) Zhang, L. F.; Eisenberg, A. Multiple morphologies and characteristics of "crew-cut" micelle-like aggregates of polystyrene-*b*-poly (acrylic acid) diblock copolymers in aqueous solutions. *J. Am. Chem. Soc.* **1996**, *118*, 3168−3181.

(2) Jenekhe, S. A.; Chen, X. L. Self-assembled aggregates of rod-coil block copolymers and their solubilization and encapsulation of fullerenes. *Science* **1998**, *279*, 1903−1907.

(3) Zubarev, E. R.; Pralle, M. U.; Li, L.; Stupp, S. I. Conversion of supramolecular clusters to macromolecular objects. *Science* **1999**, *283*, 523−526.

(4) Li, Y.; Lokitz, B. S.; McCormick, C. L. Thermally responsive vesicles and their structural "locking" through polyelectrolyte complex formation. *Angew. Chem., Int. Ed.* **2006**, *45*, 5792−5795.

(5) Mai, Y.; Eisenberg, A. Self-assembly of block copolymers. *Chem. Soc. Rev.* **2012**, *41*, 5969−5985.

(6) Ji, X.; Dong, S.; Wei, P.; Xia, D.; Huang, F. A Novel Diblock Copolymer with a Supramolecular Polymer Block and a Traditional Polymer Block: Preparation, Controllable Self-Assembly in Water, and Application in Controlled Release. *Adv. Mater.* **2013**, *25*, 5725−5729.

(7) Chi, X. D.; Ji, X. F.; Xia, D. Y.; Huang, F. A Dual-Responsive Supra-Amphiphilic Polypseudorotaxane Constructed from a Water-Soluble Pillar[7]arene and an Azobenzene-Containing Random Copolymer. *J. Am. Chem. Soc.* **2015**, *137*, 1440−1443.

(8) Wang, J. H.; Altukhov, O.; Cheng, C. C.; Chang, F. C.; Kuo, S.-W. Supramolecular structures of uracil-functionalized PEG with multi-diamidopyridine POSS through complementary hydrogen bonding interactions. *Soft Matter* **2013**, *9*, 5196−5206.

(9) Kuo, S. W.; Lee, H. F.; Huang, W. J.; Jeong, K. U.; Chang, F. C. Solid state and solution self-assembly of helical polypeptides tethered to polyhedral oligomeric silsesquioxanes. *Macromolecules* **2009**, *42*, 1619−1626.

(10) Chen, S. C.; Kuo, S. W.; Liao, C. S.; Chang, F. C. Syntheses, specific interactions, and pH-sensitive micellization behavior of poly [vinylphenol-*b*-2-(dimethylamino) ethyl methacrylate] diblock copolymers. *Macromolecules* **2008**, *41*, 8865−8876.

(11) Zhang, L.; Yu, K.; Eisenberg, A. Ion-induced morphological changes in" crew-cut" aggregates of amphiphilic block copolymers. *Science* **1996**, *272*, 1777−1779.

(12) Jain, S.; Bates, F. S. On the origins of morphological complexity in block copolymer surfactants. *Science* **2003**, *300*, 460−464.

(13) Bhargava, P.; Tu, Y. F.; Zheng, J. X.; Xiong, H. M.; Quirk, R. P.; Cheng, S. Z. D. Temperature-induced reversible morphological changes of polystyrene-*block*-poly (ethylene oxide) micelles in solution. *J. Am. Chem. Soc.* **2007**, *129*, 1113−1121.

(14) Kuo, S. W.; Tung, P. H.; Lai, C. L.; Jeong, K. U.; Chang, F. C. Supramolecular micellization of diblock copolymer mixtures mediated by hydrogen bonding for the observation of separated coil and chain aggregation in common solvents. *Macromol. Rapid Commun.* **2008**, *29*, 229−233.

(15) Chen, S. C.; Kuo, S. W.; Chang, F. C. On modulating the self-assembly behaviors of poly (styrene-b-4-vinylpyridine)/octyl gallate blends in solution state via hydrogen bonding from different common solvents. *Langmuir* **2011**, *27*, 10197−10205.

(16) Allen, C.; Han, J.; Yu, K.; Maysinger, D.; Eisenberg, A. Polycaprolactone−b-poly (ethylene oxide) copolymer micelles as a delivery vehicle for dihydrotestosterone. *J. Controlled Release* **2000**, *63*, 275−286.

(17) Förster, S.; Plantenberg, T. From Self-Organizing Polymers to Nanohybrid and Biomaterials. *Angew. Chem., Int. Ed.* **2002**, *41*, 688−714.

(18) Ramanathan, M.; Shrestha, L. K.; Mori, T.; Ji, Q.; Hill, J. P.; Ariga, K. Amphiphile nanoarchitectonics: from basic physical chemistry to advanced applications. *Phys. Chem. Chem. Phys.* **2013**, *15*, 10580−10611.

(19) Liu, J. Y.; Huang, W.; Pang, Y.; Zhu, X. Y.; Zhou, Y. F.; Yan, D. Y. The in vitro biocompatibility of self-assembled hyperbranched copolyphosphate nanocarriers. *Biomaterials* **2010**, *31*, 5643.

(20) Gao, Z.; Varshney, S. K.; Wong, S.; Eisenberg, A. Block copolymer" crew-cut" micelles in water. *Macromolecules* **1994**, *27*, 7923−7927.

DOI: 10.1021/acs.macromol.7b01516
Macromolecules 2017, 50, 7091−7101

(21) Chen, E.; Xia, Y.; Graham, M. J.; Foster, M. D.; Mi, Y.; Wu, W.; Cheng, S. Z. D. Glass transition behavior of polystyrene blocks in the cores of collapsed dry micelles tethered by poly (dimethylsiloxane) coronae in a PS-*b*-PDMS diblock copolymer. *Chem. Mater.* **2003**, *15*, 2129−2135.
(22) Bhargava, P.; Zheng, J. X.; Li, P.; Quirk, R. P.; Harris, F. W.; Cheng, S. Z. D. Self-assembled polystyrene-*block*-poly(ethylene oxide) micelle morphologies in solution. *Macromolecules* **2006**, *39*, 4880−4888.
(23) Tamami, M.; Hemp, S. T.; Zhang, K.; Zhang, M. Q.; Moore, R. B.; Long, T. E. Poly(ethylene glycol)-based ammonium ionenes containing nucleobases. *Polymer* **2013**, *54*, 1588−1595.
(24) Liu, L. Z.; Wu, L. B.; Tan, J. Y.; Wang, L.; Liu, Q.; Liu, P. W.; Liu, L. Reduction responsive thymine-conjugated biodynamers: synthesis and solution properties. *Polym. Chem.* **2015**, *6*, 3934−3941.
(25) Huang, C. W.; Mohamed, M. G.; Zhu, C. Y.; Kuo, S. W. Functional supramolecular polypeptides involving $\pi-\pi$ stacking and strong hydrogen-bonding interactions: A conformation study toward carbon nanotubes (CNTs) dispersion. *Macromolecules* **2016**, *49*, 5374−5385.
(26) Wu, Y. C.; Bastakoti, B. P.; Pramanik, M.; Yamauchi, Y.; Kuo, S. W. Multiple hydrogen bonding mediates the formation of multi-compartment micelles and hierarchical self-assembled structures from pseudo A-*block*-(B-graft-C) terpolymers. *Polym. Chem.* **2015**, *6*, 5110−5124.
(27) Huang, K. W.; Wu, Y. R.; Jeong, K. U.; Kuo, S. W. From random coil polymers to helical structures induced by carbon nanotubes and supramolecular interactions. *Macromol. Rapid Commun.* **2013**, *34*, 1530−1536.
(28) Hu, W. H.; Huang, K. W.; Chiou, C. W.; Kuo, S. W. Complementary multiple dydrogen bonding interactions induce the self-assembly of supramolecular structures from heteronucleobase-functionalized benzoxazine and polyhedral oligomeric silsesquioxane nanoparticles. *Macromolecules* **2012**, *45*, 9020−9028.
(29) Ilhan, F.; Gray, M.; Rotello, V. M. Reversible side chain modification through noncovalent interactions."Plug and play" polymers. *Macromolecules* **2001**, *34*, 2597−2601.
(30) Lee, J. C.; Litt, M. H.; Rogers, C. E. Synthesis and properties of (Alkylthio) methyl-substituted poly(oxyalkylene)s and (Alkylsulfonyl) methyl-Substituted poly(oxyalkylene)s. *Macromolecules* **1997**, *30*, 3766−3774.
(31) de Crevoisier, G.; Fabre, P.; Corpart, J. M.; Leibler, L. Switchable tackiness and wettability of a liquid crystalline polymer. *Science* **1999**, *285*, 1246−1249.
(32) Lewis, A. L.; Cumming, Z. L.; Goreish, H. H.; Kirkwood, L. C.; Tolhurst, L. A.; Stratford, P. W. Crosslinkable coatings from phosphorylcholine-based polymers. *Biomaterials* **2001**, *22*, 99−111.
(33) Huang, C. Y.; Jiang, G. Q.; Advincula, R. Electrochemical cross-linking and patterning of nanostructured polyelectrolyte−carbazole precursor ultrathin films. *Macromolecules* **2008**, *41*, 4661−4670.
(34) Ciftci, S.; Kuehne, A. J. C. Monodisperse conjugated polymer particles via Heck coupling a kinetic study to unravel particle formation in step-growth dispersion polymerization. *Macromolecules* **2015**, *48*, 8389−8393.
(35) Morin, J. F.; Leclerc, M. 2,7-Carbazole-based conjugated polymers for blue, green, and red light emission. *Macromolecules* **2002**, *35*, 8413−8417.
(36) Wu, C.; Chiu, D. T. Highly fluorescent semiconducting polymer dots for biology and medicine. *Angew. Chem., Int. Ed.* **2013**, *52*, 3086−3109.
(37) Tuncel, D.; Demir, H. V. Conjugated polymer nanoparticles. *Nanoscale* **2010**, *2*, 484−494.
(38) Cianga, L.; Bendrea, A. D.; Fifere, N.; Nita, L. E.; Doroftei, F.; Ag, D.; Seleci, M.; Timur, S.; Cianga, I. Fluorescent micellar nanoparticles by self-assembly of amphiphilic, nonionic and water self-dispersible polythiophenes with "hairy rod" architecture. *RSC Adv.* **2014**, *4*, 56385−56405.
(39) Huang, C. W.; Chang, F. C.; Chu, Y. L.; Lai, C. C.; Lin, T. E.; Zhu, C. Y.; Kuo, S. W. A solvent-resistant azide-based hole injection/transporting conjugated polymer for fluorescent and phosphorescent light-emitting diodes. *J. Mater. Chem. C* **2015**, *3*, 8142−8151.
(40) Huang, C. W.; Wu, P. W.; Su, W. H.; Zhu, C. Y.; Kuo, S. W. Stimuli-responsive supramolecular materials: photo-tunable properties and molecular recognition behavior. *Polym. Chem.* **2016**, *7*, 795−806.
(41) Wu, Y. C.; Wu, Y. S.; Kuo, S. W. Bioinspired photo-core-crosslinked and noncovalently connected micelles from functionalized polystyrene and poly(ethylene oxide) homopolymers. *Macromol. Chem. Phys.* **2013**, *214*, 563−571.
(42) Wu, C.; Szymanski, C.; McNeill, J. Preparation and encapsulation of highly fluorescent conjugated polymer nanoparticles. *Langmuir* **2006**, *22*, 2956−2960.
(43) Sartorius, J.; Schneider, H. J. A general scheme based on empirical increments for the prediction of hydrogen-bond associations of nucleobases and of synthetic host−guest complexes. *Chem. - Eur. J.* **1996**, *2*, 1446−1452.
(44) Binder, W. H.; Zirbs, R. Supramolecular polymers and networkswith hydrogen bonds in the main-and side-chain. *Adv. Polym. Sci.* **2006**, *207*, 1−78.
(45) Zipfel, W. R.; Williams, R. M.; Webb, W. W. Nonlinear magic: multiphoton microscopy in the biosciences. *Nat. Biotechnol.* **2003**, *21*, 1369−1377.
(46) Wu, C. F.; Szymanski, C.; Cain, Z.; McNeill, J. Conjugated polymer dots for multiphoton fluorescence imaging. *J. Am. Chem. Soc.* **2007**, *129*, 12904−12905.
(47) Chennoufi, R.; Bougherara, H.; Gagey-Eilstein, N.; Dumat, B.; Henry, E.; Subra, F.; Mahuteau-Betzer, F.; Tauc, P.; Teulade-Fichou, M. P.; Deprez, E. Differential behaviour of cationic triphenylamine derivatives in fixed and living cells: triggering and imaging cell death. *Chem. Commun.* **2015**, *51*, 14881−14884.
(48) Chennoufi, R.; Bougherara, H.; Gagey-Eilstein, N.; Dumat, B.; Henry, E.; Subra, F.; Bury-Moné, S.; Mahuteau-Betzer, F.; Tauc, P.; Teulade-Fichou, M. P.; Deprez, E. Mitochondria-targeted triphenylamine derivatives activatable by two-photon excitation for triggering and imaging cell apoptosis. *Sci. Rep.* **2016**, *6*, 21458.

DOI: 10.1021/acs.macromol.7b01516
Macromolecules 2017, 50, 7091−7101